Journal of Statistical Physics, Vol. 77, Nos. 1/2, 1994

Statistical Model of the Habit and Arrangement of Mineral Crystals in the Collagen of Bone

Peter Fratzl[1,2]

Received August 31, 1993; final January 19, 1994

Randomly colored space tesselations are considered as models for the mineral/organic structure of bone. First, it is shown that the structure function for such models is always proportional to the average form factor of the individual tiles and hence independent of the mineral density in the sample. Then the structure function is calculated for three such models: for model 1, based on a hexagonal, and model 2, on a Poisson–Voronoi tesselation of the plane and for model 3, based on a random tesselation of the line. These results are compared to experimental structure functions measured by small-angle scattering and excellent agreement is obtained between model 2 and the bone from mice and rats, as well as between model 3 and calcified turkey leg tendon. Divergent conclusions following recent experiments by small-angle x-ray scattering and by electron microscopy are discussed in the light of these structural models and an explanation is proposed which might remove the discrepancy.

KEY WORDS: Bone; collagen; Voronoi tesselations; small-angle scattering; structure function; calcified tissue.

1. INTRODUCTION

The structure of bone as a mineral/organic compound is of primary importance for the mechanical properties of the skeleton. The structural relationships between the components, mostly hydroxyapatite crystals and collagen,[1-3] are still not fully elucidated, probably because their size is only in the order of nanometers. For this reason a large research effort is currently devoted to the study of bone using high-resolution methods, such as electron microscopy (EM),[4-9] x-ray,[10-15] and neutron[16,17] scattering and other techniques.[18,19]

Dedicated to Prof. Oliver Penrose on the occasion of his 65th birthday.

[1] Institut für Festkörperphysik der Universität Wien, A-1090 Vienna, Austria.

[2] Ludwig Boltzmann-Institut für Osteologie, Hanusch Krankenhaus, Vienna, Austria.

0022-4715/94/1000-0125$07.00/0

The collagen/mineral compound consists of fibrils of parallel molecules with mineral phase embedded inside. There is a general agreement that the mineral crystals are elongated particles, with their long dimension parallel to the molecules in the collagen fibril. Recently, a parallel arrangement of platelike crystals was revealed in calcified turkey leg tendon by three-dimensional reconstruction using high-voltage EM tomography.[9] The situation is less clear for other types of bone, where either plate-shaped[6,7,4] or needle-shaped[20,12,21] crystals were suggested from studies by electron microscopy and other more indirect techniques. In particular, a clear difference was recently observed in the small-angle x-ray scattering (SAXS) from calcified turkey leg tendon on one hand and from mouse or rat bone on the other. While the SAXS results for turkey tendon indeed agree with the existence of thin parallel mineral platelets, the results for mouse bone rather suggest a more irregular arrangement built up by (sometimes adjacent) needlelike objects, i.e., by crystal units where two dimensions are much smaller than the third.[13]

Although, unlike electron microscopy, SAXS does not provide direct images of the structure, it has the advantage that the material can be studied virtually without sample preparation, i.e., with the lowest possible danger of altering the original structure by the preparation process. Moreover, very accurate average values can be obtained by SAXS for a few parameters (or "invariants"[22-24]), such as the total volume and interface of the crystals. As the structure function measured by SAXS is just proportional to the squared absolute value of the Fourier transform of the electron density in the sample, EM and SAXS data should simply correspond by Fourier transformation. Unfortunately, the phase information is lost in the scattering process and for a direct comparison of EM with SAXS data one must rely on structural models to fit the SAXS results.

An extensive study of the correspondence between EM pictures and SAXS spectra has been carried out in recent years for the morphology of two-phase structures formed by spinodal decomposition,[25-28] where precipitates of a given phase grow and coarsen within a different matrix phase. This is not unlike the case of mineralized collagen, which can be expected to form by the precipitation of mineral particles within the collagen matrix. Nevertheless, the structure functions measured for spinodal decomposition[29,30,28] and for bone[13,14] are completely different. In particular, the structure function for spinodal decomposition exhibits a maximum at finite wavevectors, which is absent for bone. A recently proposed model,[13] based on rod-shaped mineral crystals distributed randomly within the collagen matrix, is able to explain at least this absence of the maximum. A model reproducing the SAXS spectra for bone quantitatively is, however, still lacking.

In the following, the author calculates the structure function for several models, based on space tesselations, i.e., a complete subdivision of space into tiles, where it is supposed that some of the tiles correspond to mineral phase and others to organic substance (mainly collagen). The essential hypothesis, which will make the calculations tractable, is that the mineral phase is distributed randomly among the tiles. First, it is shown that for such models the total scattering is just proportional to the scattering from an individual tile and is therefore independent of the mineral density. Moreover, the structure function constructed using a *two-dimensional* Poisson–Voronoi tesselation is shown to reproduce exactly the SAXS curves from bones of mice, rats, and dogs. A good representation for the SAXS from mineralized turkey leg tendon is, on the contrary, obtained with a structure of platelike mineral crystals based on a *one-dimensional* random tesselation. Typical pictures for the mineral distribution within these models are compared to EM results from the literature.

2. DESCRIPTION OF THE MODELS FOR MINERALIZED COLLAGEN

As the mineral crystals are elongated objects parallel to the collagen molecules in the fibril, only a two-dimensional section across the fibril needs to be considered. Indeed, if a planar structure is supposed to be continued into the third dimension by simple translation of the plane, the three-dimensional (spherically averaged) structure function S_3 is[28]

$$S_3(k) = \frac{\pi}{k} S_2(k) \tag{1}$$

where S_2 is the spherically averaged structure function in the plane.

Model 1. The first model, already proposed in ref. 13, consists of a hexagonal lattice where the tiles are colored black in a random fashion. The black regions symbolize the mineral, whereas the white regions are occupied by collagen. The three-dimensional structure is obtained by translating this planar structure along the direction perpendicular to the plane. Figure 1 shows a realization of this model. In Fig. 1a the hexagonal lattice is drawn and in Fig. 1b 20% of the tiles are colored black, 40% in Fig. 1c, and 60% in Fig. 1d. Figure 1b, for instance, could be a cross section through a collagen fibril with a mineral content of 20%. Each black tile has to be imagined as a hexagonal rod oriented perpendicularly to the figure. Most crystals in Fig. 1a are therefore needlelike, but in the upper part of the figure an almost platelike object can be seen, which was formed by chance due to the random coloring of the tiles. This model is somewhat

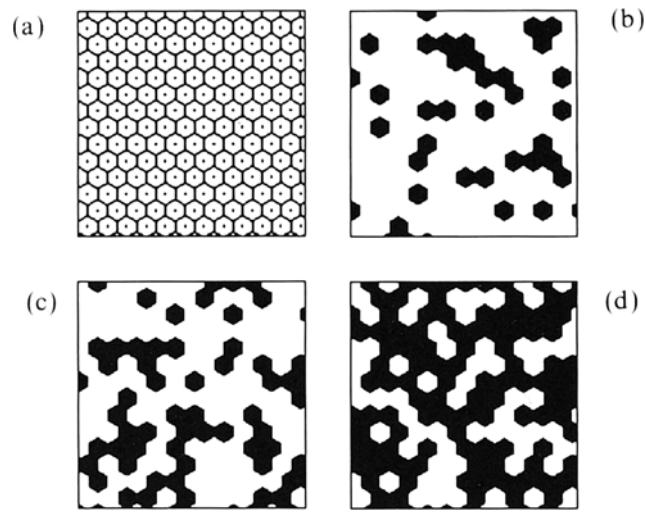

Fig. 1. (a) A hexagonal tesselation of the plane. The dots indicate the centers of the hexagons. (b–d) 20%, 40%, and 60% of the hexagons, respectively, were chosen at random and colored black. The rest were left white.

unrealistic, because of the regular shape of the tiling. The collagen fibril itself is known to have only a liquidlike ordering within the plane shown in Fig. 1,[15] so that a strictly periodic arrangement of the crystals is also not to be expected.

Model 2. A more irregular space tiling is achieved with the Poisson–Voronoi tesselation. This is constructed by throwing points at random onto the plane (see the points in Fig. 2a). The polygonal region that lies nearer to a given point than to any other is assigned to that point. This creates the tesselation shown in Fig. 2a. The polygons are then colored at random, giving structures as in Fig. 2b (for 20% of mineral), Fig. 2c (40%), and Fig. 2d (60%). Again each black tile corresponds to a cylinder with its axis perpendicular to the paper. The structure of the mineral phase is now very irregular, showing mostly needlelike objects at low densities (Fig. 2b), but platelike and even more complicated patterns at higher densities (Figs. 2c and 2d).

The two previous models are based on a planar tesselation into tiles of finite size. The typical elementary object is therefore needlelike. These models are intended to describe the structure of bone from rats and mice.[14] To have a model for a distribution of parallel plates as proposed, e.g., for the structure of calcified turkey leg tendon,[6, 9, 14] one-dimensional

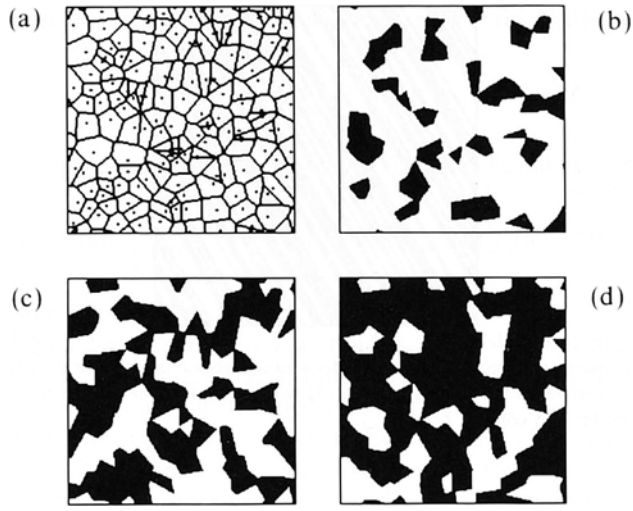

Fig. 2. (a) A Poisson–Voronoi tesselation of the plane. The dots indicate the Poisson points. (b–d) 20%, 40%, and 60% of the Voronoi polygons, respectively, were chosen at random and colored black. The rest were left white.

tesselations of the line are also considered. In analogy to Eq. (1), the three-dimensional structure function follows from the one-dimensional one by

$$S_3(k) = \frac{2\pi}{k^2} S_1(k) \tag{2}$$

Model 3. Within the plane normal to the fibril direction, a line is chosen at random and this line is subdivided into intervals with length l according to the probability distribution $p(l)\,dl$. The interval lengths are supposed independent. A two-dimensional picture similar to Figs. 1 and 2 is obtained by drawing stripes perpendicularly to the intervals and by coloring the stripes at random. Figure 3 shows such a structure of parallel plates with a mineral density of 50% and where the probability distribution of interval lengths has been chosen

$$p(l)\,dl = \left(\frac{n}{l_0}\right)^n \frac{l^{n-1}}{(n-1)!} e^{-nl/l_0} \tag{3}$$

with $n = 4$ and l_0 the average plate thickness.

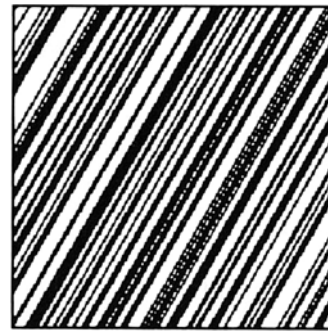

Fig. 3. Succession of plates corresponding to a randomly colored linear tesselation with an interval length distribution according to Eq. (3) with $n=4$. Fifty percent of the intervals were chosen at random and colored black.

3. RANDOMLY FILLED SPACE TESSELATIONS

Consider a tesselation of ν-dimensional space into separate regions V_n so that

$$\bigcap_{n=1}^{N} V_n = 0, \qquad W_N = \bigcup_{n=1}^{N} V_n \tag{4}$$

and $\lim_{N\to\infty}(W_N)$ is covering the whole space. It is further supposed that each of the tiles V_n may be either filled with mineral or with organic substance. A parameter u_n is defined to be $=1$ if there is mineral phase inside the tile V_n and $=0$ otherwise. Moreover, an average occupation of the tiles is defined by

$$\bar{u} = \lim_{N\to\infty} \frac{1}{N} \sum_{n=1}^{N} u_n \tag{5}$$

and a volume fraction of mineral phase by

$$\phi = \lim_{N\to\infty} \frac{1}{|W_N|} \sum_{n=1}^{N} u_n |V_n| \tag{6}$$

the vertical bars denoting the volume of the tile. The spherically averaged structure function $S_\nu(k)$ for this model can be calculated by[28]

$$S_\nu(k) = \lim_{N\to\infty} \left[\frac{1}{|W_N|} \left\langle \left| \sum_{n=1}^{N} \int_{V_n} (u_n - \bar{u})\, e^{i\mathbf{k}\cdot\mathbf{r}}\, d^\nu\mathbf{r} \right|^2 \right\rangle \right] \tag{7}$$

where the brackets denote spherical average and $k = |\mathbf{k}|$. With the notation

$$f_n(\mathbf{k}) = \int_{V_n} e^{i\mathbf{k}\cdot\mathbf{r}}\, d^\nu \mathbf{r} \tag{8}$$

and using the properties (4), the structure function becomes

$$S_\nu(k) = \lim_{N\to\infty} \left[\frac{1}{|W_N|} \left\langle \sum_{n,m=1}^{N} (u_n - \bar{u})(u_m - \bar{u})\, f_n(\mathbf{k})\, f_m^*(\mathbf{k}) \right\rangle \right] \tag{9}$$

where the star denotes the complex conjugate.

Now let us consider the $\{u_n\}$ as random variables that may be equal to either 0 or 1. The simplest such model is obtained when the mineral is supposed to be randomly distributed over the tiles. In this case u_n and u_m are uncorrelated if $m \neq n$ and $\bar{u} = \phi$ [see Eqs. (5) and (6)]. Separating the sum in Eq. (9) into a term for $n = m$ and another for $n \neq m$, we find that the second term vanishes because u_n and u_m are uncorrelated and the average of u_n is just $\bar{u} = \phi$. Moreover, for all n, $u_n^2 = u_n$ (because u_n can only be equal to 0 or 1) and

$$\overline{(u_n - \bar{u})^2} = \overline{u_n^2} - \bar{u}^2 = \phi(1-\phi) \tag{10}$$

With this simplification, Eq. (9) becomes

$$S_\nu(k) = \phi(1-\phi)\, \tilde{S}_\nu(k)$$

where

$$\tilde{S}_\nu(k) = \lim_{N\to\infty} \left[\frac{1}{|W_N|} \left\langle \sum_{n=1}^{N} |f_n(\mathbf{k})|^2 \right\rangle \right] \tag{11}$$

is the average structure function of a individual tile of the tesselation. The remarkable consequence is that, regardless of the density of mineral in the sample, the scattering will be proportional to the same function, which is the average scattering from the tiles in the tesselation. Consequently, if the individual tiles have a needlelike shape, the total scattering function will be that of a needlelike object, and if the individual tiles are plate-shaped, this will also be reflected directly in the total structure function.

4. INVARIANTS OF THE STRUCTURE FUNCTION

There are a few general results about the structure function of a two-phase structure, mostly due to Guinier and Fournet[22] and Porod,[23] which are of importance for the present problem and are recalled here.

4.1. Porod's Law

If there is a sharp interface between the two phases (mineral and organic) then the structure function S_ν should decay at large k according to Porod's law[23, 22]

$$S_\nu(k) \approx \frac{P_\nu \sigma}{k^{\nu+1}} \tag{12}$$

where P_ν is a constant and σ the total *interface area* per unit volume in ν-dimensional space. With the definition (7) of S_ν, one has

$$P_3 = 2\pi, \qquad P_2 = 2, \qquad P_1 = 1 \tag{13}$$

Indeed, $S_3(k)$ measured for bone by SAXS is usually found to follow Porod's law.[13, 14]

The *volume fraction* ϕ of the precipitates is related to the integral intensity by[28]

$$\int_0^\infty k^{\nu-1} S_\nu(k)\, dk = \pi\phi(1-\phi) P_\nu \tag{14}$$

This allows us to define an average correlation length of the two-phase structure by[23, 25, 26, 28]

$$T = 4\frac{\phi(1-\phi)}{\sigma} = \frac{4}{\pi P_\nu \sigma} \int_0^\infty k^{\nu-1} S_\nu(k)\, dk \tag{15}$$

The parameter T has a simple interpretation for a structure based on space tesselations as described in Section 3. Then, for $\nu = 3$, if the mineral phase is supposed to consist of individual crystals of size $a \leqslant b \leqslant c$,

$$T \approx \frac{2abc}{ab + bc + ca} \tag{16}$$

For needlelike crystals ($a, b \ll c$), this gives $T \approx (2ab)/(a+b)$, and in particular for $a = b \ll c$, $T \approx a$. For platelike crystals ($a \ll b, c$) it gives $T \approx 2a$. Consequently, T can be interpreted as a measure of the smallest dimension (i.e., the average thickness) of the mineral crystals in bone.[13, 14]

4.2. Guinier's Law

Whereas the average thickness T can be determined without any model assumptions about the two-phase structure, another characteristic

length, the Guinier radius,[22] can only be determined for very small ϕ or within a model as described in Section 3. Considering a space tesselation into tiles of *finite size*, we can develop the structure function Eq. (11) to second order for small k as follows.

For convenience, a function $\chi_n(\mathbf{r})$ is defined such that $\chi_n(\mathbf{r})=1$ if $\mathbf{r}$ is inside V_n and $=0$ otherwise. Introducing $\mathbf{r}_n$, we define the center of mass of V_n as

$$\mathbf{r}_n=\frac{1}{|V_n|}\int \mathbf{r}\chi_n(\mathbf{r})\,d^\nu\mathbf{r} \tag{17}$$

Equation (11) becomes

$$\begin{aligned}\tilde{S}_\nu(k)&=\lim_{N\to\infty}\left\{\frac{1}{|W_N|}\left\langle\sum_{n=1}^{N}\left|\int\left[1+i\mathbf{k}\cdot\mathbf{s}-\frac{1}{2}(\mathbf{k}\cdot\mathbf{s})^2+o(\mathbf{k}^2)\right]\right.\right.\right.\\&\quad\left.\left.\left.\times\chi_n(\mathbf{r}_n+\mathbf{s})\,d^\nu\mathbf{s}\right|^2\right\rangle\right\}\\&=\lim_{N\to\infty}\left\{\frac{1}{|W_N|}\sum_{n=1}^{N}\left[|V_n|^2-|V_n|\int\langle(\mathbf{k}\cdot\mathbf{s})^2\rangle\,\chi_n(\mathbf{r}_n+\mathbf{s})\,d^\nu\mathbf{s}\right]\right\}+o(k^2)\\&=A_g^2\left(1-\frac{k^2}{\nu}R_g^2\right)+o(k^2)\end{aligned} \tag{18}$$

where A_g is an average volume of the tiles:

$$A_g^2=\lim_{N\to\infty}\left(\frac{1}{|W_n|}\sum_{n=1}^{N}|V_n|^2\right) \tag{19}$$

and R_g an average radius of gyration of the tiles:

$$R_g^2=\lim_{N\to\infty}\left\{\frac{1}{|W_N|}\sum_{n=1}^{N}\left[|V_n|\int s^2\chi_n(\mathbf{r}_n+\mathbf{s})\,d^\nu\mathbf{s}\right]\right\}\Big/A_g^2 \tag{20}$$

In the case of a randomly colored tesselation, one therefore obtains a generalized Guinier law[22] in the form

$$S_\nu(k)\approx A_g^2 e^{-k^2R_g^2/\nu}\qquad\text{for small values of } k \tag{21}$$

For a three-dimensional structure obtained by translating a planar tesselation (models 1 and 2), the Guinier law becomes [using Eq. (1)]

$$S_3(k)\approx\frac{\pi}{k}A_g^2 e^{-k^2R_g^2/2} \tag{22}$$

where R_g is the average radius of gyration of the planar tile. For a structure obtained from a linear tesselation [model 3, using Eq. (2)]

$$S_3(k) \approx \frac{2\pi}{k^2} A_g^2 e^{-k^2 R_g^2} \tag{23}$$

where $2R_g$ is the average thickness of the intervals on the line according to Eq. (20).

5. CALCULATION OF THE STRUCTURE FUNCTIONS

The results will be presented in terms of a scaled structure function $F(q)$, where

$$q = kT \qquad \text{and where} \qquad \int_0^\infty 4\pi q^2 F(q)\, dq = 1$$

With the use of Eq. (14), this means

$$F(q) = S_3(q/T)/[8\pi^3 T^3 \phi(1-\phi)] \tag{24}$$

5.1. Structure Function for Model 1

As all the elementary tiles in the (planar) tesselation are identical hexagons, the function $|f_n(\mathbf{k})|^2$ defined by Eq. (8) will be independent of n and, say, equal to $|f^{\mathrm{H}}(\mathbf{k})|^2$. Consequently, the crystal thickness T [Eq. (15)] will be equal to $T = 4\,|V^{\mathrm{H}}|/|S^{\mathrm{H}}|$, where $|V^{\mathrm{H}}|$ and $|S^{\mathrm{H}}|$ are the surface and the perimeter length of the hexagon (see Fig. 4). It results that

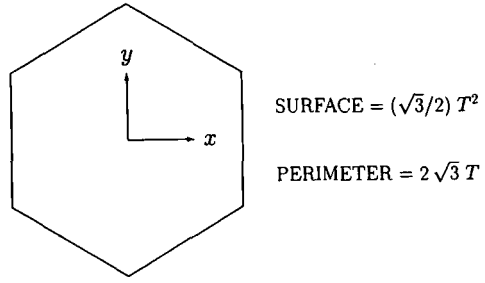

Fig. 4. Orientation of the hexagon for the calculation of F^{H}.

T is just the distance between two parallel sides of the hexagon, as shown in Fig. 4. The radius of gyration as defined in Eq. (20) is related to T by

$$2R_g = \frac{\sqrt{5}}{3} T \tag{25}$$

Combining Eqs. (1), (11), and (24), we find that the scaled structure function F^{H} of the hexagon model (model 1) becomes

$$F^{\mathrm{H}}(q) = \frac{1}{8\pi^3 \sqrt{3}\, qT^4} \int_0^{2\pi} \left| f^{\mathrm{H}}\left(\frac{\mathbf{q}}{T}\right)\right|^2 d\theta \qquad \text{where} \quad \mathbf{q} = \begin{pmatrix} q\cos\theta \\ q\sin\theta \end{pmatrix} \tag{26}$$

Defining an x and a y direction as shown in Fig. 4, one gets

$$f^{\mathrm{H}}(\mathbf{q}/T) = \int_{V^{\mathrm{H}}} e^{i\mathbf{q}\cdot\mathbf{r}/T}\, d^2\mathbf{r}$$

with V^{H} defined by (see Fig. 4)

$$|2x| \leqslant T, \qquad |x + y\sqrt{3}| \leqslant T, \qquad |x - y\sqrt{3}| \leqslant T$$

A simple calculation shows that

$$f^{\mathrm{H}}\left(\frac{\mathbf{q}}{T}\right) = \frac{\sqrt{3}}{2} T^2 \frac{k_1 \cos k_1 + k_2 \cos k_2 - k_3 \cos k_3}{6k_1 k_2 k_3} \tag{27}$$

where

$$k_1 = \frac{q}{\sqrt{3}} \sin\left(\theta - \frac{\pi}{3}\right), \qquad k_2 = \frac{q}{\sqrt{3}} \sin\left(\theta + \frac{\pi}{3}\right), \qquad k_3 = \frac{q}{\sqrt{3}} \sin\theta$$

Inserting this into Eq. (26), one obtains an expression suitable for numerical computation. Note that F^{H} is a function of q only, independent of T.

5.2. Structure Function for Model 2

Model 2 is based on a Voronoi tesselation of the plane. Such tesselations have often been used as a model for natural phenomena in a variety of fields, such as astrophysics, geography, geology, materials science, cell biology, ecology, and others (for references, see ref. 31, p. 260). In particular, Voronoi tesselations of three-dimensional space have been used to describe the morphology of two-phase systems, such as microemulsions[32] and catalysts.[33] In these works, the structure function was evaluated for the three-dimensional tesselation. Model 2 for bone is based on a two-

dimensional tesselation and the structure function will be evaluated here along the lines of the derivation for the three-dimensional case.[32]

General results about Poisson–Voronoi tesselations,[31] allow us to calculate immediately the average crystal thickness T defined in (15). Calling c the density of the Poisson process, i.e., the number of points thrown at random per unit surface, we have that the average perimeter of the typical Voronoi polygon is $4/\sqrt{c}$ and its average surface $1/c$.[31] Consequently,

$$T = \frac{1}{\sqrt{c}} \tag{28}$$

Using Eqs. (1), (11), and (24), we obtain the scaled structure function F^{V} for model 2

$$F^{V}(q) = (1/8\pi^2 T^2 q)\, \tilde{S}_2^{V}(q/T) \tag{29}$$

To calculate the structure function $\tilde{S}_2^{V}(k)$ for the average tile in the two-dimensional Poisson–Voronoi tesselation, we use the correlation function $\gamma(r)$,[32] which was introduced by Porod,[23]

$$\tilde{S}_2^{V}(k) = \int_0^{\infty} 2\pi r \gamma(r)\, J_0(kr)\, dr \tag{30}$$

where

$$\phi(1-\phi)\,\gamma(r) \equiv \lim_{N\to\infty} \left[\frac{1}{|W_N|} \left\langle \int_{W_N} (u(\mathbf{s}) - \bar{u})(u(\mathbf{r}+\mathbf{s}) - \bar{u})\, d^2\mathbf{s} \right\rangle \right] \tag{31}$$

where the function $u(\mathbf{r}) \equiv u_n$ for $\mathbf{r} \in V_n$. Due to the random coloring of the tiles, the integrand in this expression vanishes as soon as the two points $\mathbf{s}$ and $\mathbf{r}+\mathbf{s}$ are not within the same Voronoi polygon. Consequently,[32]

$$\gamma(r) = c \int \exp[-c\tilde{S}(\mathbf{r}, \mathbf{s})]\, d^2\mathbf{s} \tag{32}$$

where $\tilde{S}(\mathbf{r}, \mathbf{s})$ is the union of two circles with the centers at a distance $r = |\mathbf{r}|$ and with radii given by $|\mathbf{s}|$ and by $|\mathbf{s}+\mathbf{r}|$. This surface is $\tilde{S}(\mathbf{r}, \mathbf{s}) = r^2 S(u, \theta)$, where

$$S(u, \theta) = u^2(\pi - \theta + \tfrac{1}{2}\sin 2\theta) + v^2(\psi - \tfrac{1}{2}\sin 2\psi) \tag{33}$$

with

$$u = \frac{|\mathbf{s}|}{r}, \qquad \cos\theta = -\frac{\mathbf{s}\cdot\mathbf{r}}{sr}, \qquad v = (u^2 + 1 - 2u\cos\theta)^{1/2}$$

$$\cos\psi = \frac{u\cos\theta - 1}{v}$$

Inserting this into Eqs. (32), (30), and (29), we obtain

$$F^{V}(q) = \frac{1}{2\pi q} \int_0^\infty u\,du \int_0^\pi d\theta \int_0^\infty x^3 J_0(qx)\, e^{-x^2 S(u,\theta)}\, dx$$

$$= \frac{1}{16\pi q} \int_0^\infty u\,du \int_0^\pi d\theta \frac{4S(u,\theta) - q^2}{[S(u,\theta)]^3}\, e^{-q^2/[4S(u,\theta)]} \tag{34}$$

which depends on q only. This expression can be used for a numerical evaluation of F^{V}.

Finally, the average radius of gyration, Eq. (20), of the Poisson–Voronoi tiles can be determined by an expansion of F^{V} in powers of q for small q. Indeed, a development to the second order yields

$$F^{V}(q) \approx \frac{\mu_0}{4\pi}\frac{1}{q} - \frac{\mu_1}{8\pi} q \approx \frac{\mu_0}{4\pi q}\, e^{-q^2\mu_1/(2\mu_0)} \tag{35}$$

where

$$\mu_j = \int_0^\infty u\,du \int_0^\pi d\theta\, [S(u,\theta)]^{-(j+2)}$$

and by comparison with Eq. (21)

$$2R_g = 2\left(\frac{\mu_0}{\mu_1}\right)^{1/2} T \approx 1.072T \tag{36}$$

5.3. Structure Function for Model 3

Starting with Eq. (11), one gets for the linear tesselation (model 3)

$$\tilde{S}_1^{L}(k) = \frac{1}{l_0} \int_0^\infty p(l)\, dl \left| \int_0^l e^{ikr}\, dr \right|^2$$

Replacing $p(l)$ by its value in Eq. (3) and carrying out the integral, we obtain

$$\tilde{S}_1^{L}(k) = \frac{2}{k^2 l_0}\left[1 - \frac{\cos[n \arctan(l_0 k/n)]}{[1 + (l_0 k/n)^2]^{n/2}}\right] \tag{37}$$

From Eq. (15) it follows that the parameter T is equal to $2l_0$. Together with Eq. (2) and (24) one obtains the scaled structure function for this model

$$F^{L}(q) = \frac{1}{\pi^2 q^4}\left[1 - \frac{\cos[n \arctan(q/2n)]}{[1 + (q/2n)^2]^{n/2}}\right] \tag{38}$$

which is again independent of T.

6. DISCUSSION AND CONCLUSION

Statistical models of the habit and arrangement of mineral crystals in bone have been studied and the corresponding small-angle scattering patterns calculated. The results shall now be compared to the SAXS effectively measured for mouse bone[13] and for mineralized turkey leg tendon.[14]

In both cases, the diffuse small-angle scattering intensity was concentrated in the equatorial plane normal to the fibril axis.[13,14] To account for this observation, the crystals (whether plate- or needlelike) were supposed parallel to the collagen molecules for all models considered here. Moreover, diffraction spots had been observed in the axial direction of the collagen for both tissues (mouse bone[13] and turkey tendon[14]), which means that the crystals are in register with the 64-nm periodicity of collagen and hence located predominantly inside the gap zone of the collagen fibril.[16] The pictures (Figs. 1–3) drawn for the mineral arrangement should therefore be regarded as highly magnified cross sections of one fibril perpendicular to the axial direction of the collagen and located inside the gap region.

For a quantitative comparison, scaled structure functions $F(q)$ have been obtained for three structural models, based on randomly filled space tesselations. Due to the rescaling [Eq. (24)] with the crystal thickness parameter [Eq. (15)] there is no free parameter in models 1 and 2, which correspond to structures formed by needlelike mineral crystals embedded into a collagen matrix (Figs. 1 and 2). There is just one parameter n in model 3, which describes parallel platelike mineral crystals in the collagen fibril. n is a measure for the width of the distribution of crystal thicknesses; the larger n, the narrower the distribution. In the limit when $n \to \infty$, all crystals have exactly the same width. As the parameter T can be determined directly also for experiment data [see Eq. (15) and refs. 13 and 14], a parameter-free comparison between the models and the measurements is possible. The precise meaning of the thickness parameter T within the three models is tabulated in Table I, confirming the qualitative interpretation of T given after Eq. (15).

Table I. Parameters Characterizing the Mineral Crystals as a Function of Crystal Thickness T [Eq. (15)]

	Model 1	Model 2	Model 3
Radius of gyration of the needle cross section	$0.75(T/2)$	$1.07(T/2)$	—
Average surface of the needle cross section	$0.87T^2$	T^2	—
Average perimeter of the needle cross section	$3.46T$	$4T$	—
Average plate thickness	—	—	$T/2$

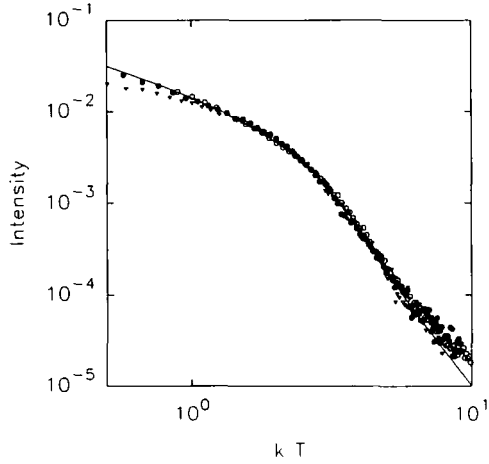

Fig. 5. Plot of F^{V} (full line) as given by Eq. (29) compared to measured scaled structure functions for rat (full circles), mouse (triangles), and dog (open circles) femur (data from ref. 14).

The comparison between the models and experiment data is carried out in Figs. 5–7. Figure 5 shows the data for the measured structure function of bone from rats, mice, and dogs, taken from ref. 14, together with model 2 [Eq. (29)]. Although there is no free parameter in the model, the agreement is almost perfect. Figure 6 shows the data for mineralized turkey

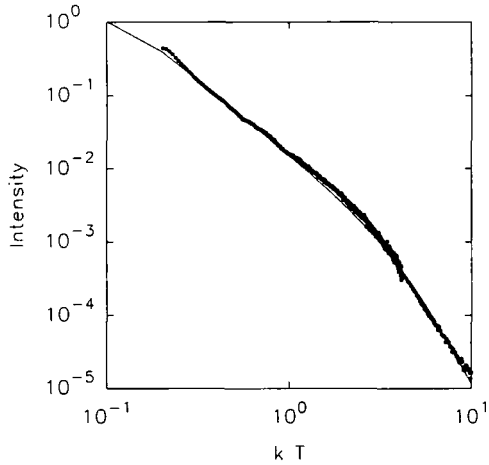

Fig. 6. Plot of F^{L} (full line) as given by Eq. (38) with $n=4$ compared to the measured scaled structure function for calcified turkey leg tendon (data from ref. 14).

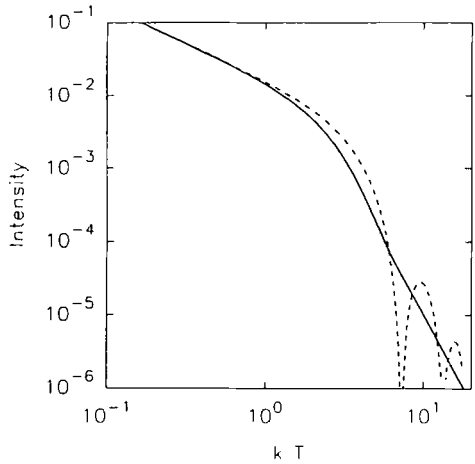

Fig. 7. Comparison of F^V (full line) given by Eq. (29) to F^H (broken line) given by Eq. (26). Note the oscillations of F^H at large $q = kT$, due to the regular shape of the hexagonal tile.

leg tendon (from ref. 14) together with model 3 (with $n = 4$). Again the agreement is remarkably good. Models 1 and 2 are compared in Fig. 7. The curves are quite similar for small values of q, but model 1 has unrealistic oscillations at large q, due to the regularity of the hexagonal tesselation. It is clear that model 1 reproduces the essential features at small q, but would not fit the data in Fig. 5 at large q.

Figures 5 and 6 show that model 2 gives an excellent account of the structure function from rat and mouse bone, and model 3 that of mineralized turkey tendon. Hence, Figs. 2 and 3, respectively, show an arrangement of mineral crystals in agreement with the SAXS data for these two types of mineralized tissue. All pictures correspond to a cross section of the fibril perpendicular to the axial direction of collagen, where the mineral phase is shown in black. Although contributions to the SAXS from mineral crystals located outside the collagen fibrils cannot be excluded, the fact that the crystals are in both cases mostly parallel to collagen molecules and appear with a 64-nm axial periodicity indicates that most of the scattering is due to mineral inside the fibril. Hence, Figs. 2 and 3 can be understood as cross sections through the gap zone of the mineralized collagen fibril in the case of rat bone and turkey tendon, respectively.

In the case of mineralized turkey leg tendon (Fig. 3), the structure which best describes the SAXS data consists of parallel mineral plates. However, the distance between these plates cannot be constant throughout the sample, because this would lead to maximum in the equatorial scatter-

ing, which is not observed.[14] The present model calculations rather suggest a considerable variation of the distance between the plates. This indicates that the number of layers of collagen molecules between crystals must be variable, in contrast to earlier models.[6] This might be linked to the fact directly observed, e.g., in fish bone,[8] that the mineralization proceeds at considerably different speed in adjacent fibrils, leading to fluctuations of the mineral density and hence of the distance between mineral crystals.

In the case of mouse or rat bone, a model built with parallel platelets is unable to reproduce the SAXS data. Perfect agreement is obtained, however, with a structure similar to the one shown in Fig. 2, built of individual, rather needlelike units. At low density (Fig. 2b), one can see individual needles of varying shapes; at higher densities (Fig. 2c) these needles agglomerate to more complicated structures, which can frequently have the character of interconnected plates. In fact, the main difference from model 3 is the interconnectivity of the crystals. Connectivity of the mineral is indeed essential to explaining the common observation that bone does not fall into pieces even after the removal of all the collagen. Moreover, the change from individual needles in Fig. 2b to a more complicated interconnected structure (which in many respects looks similar to interconnected plates with varying orientation) could well correspond to the fact that by means of electron microscopy individual needles are mainly observed in the early stages of mineralization, whereas they appear rather platelike in more strongly mineralized tissue.[1]

Another interesting aspect is the absence of an interference maximum in the structure function, as usually observed for morphologies grown by spinodal decomposition[25, 26, 28–30] or in x-ray scattering from macromolecular solutions. The *mathematical* reason is the random distribution of the mineral on the tiles of a space tesselation (Section 3), the *physical* reason must be inherent in the nucleation process of the second phase. The reason for the appearence of the interference maximum in the case of spinodal decomposition is the conservation of matter during nucleation, growth, and coarsening.[28] This means that, due to diffusion limitations, material cannot be exchanged over large distances. Therefore, close to a precipitate there is a low probability of finding another one because all the material has already been used up by the first precipitate. Already Guinier and Fournet[22] introduced the concept of "depletion zones" around precipitates to be responsible for the interference peak in the structure function. No such depletion zone is expected during nucleation and growth of the calcium phosphate precipitates inside collagen. Indeed, the small calcium and phosphate ions are transported in aqueous solution, a process which is orders of magnitude faster than solid-state diffusion. This removes

effectively the conservation constraint and no correlations in the positions of the mineral precipitates in the equatorial plane (i.e., the cross section through the gap zone of the fibril) and therefore no maximum in the structure function are induced within the equatorial plane.

In conclusion, the structure function has been calculated for models based on randomly colored space tesselations, and excellent agreement is obtained with SAXS data for different mineralized tissues. The resulting pictures for the mineral structure show parallel plates for turkey leg tendon. For the bones of mice and rats perfect agreement with SAXS data is obtained by a structure built by needlelike units. With increasing mineral density, the individual needles merge into plates of various orientations to give a mineral structure with high interconnectivity. Although this structure still needs to be confirmed by EM tomography, such as used in the case of turkey leg tendon,[9] the present model may explain some of the diverging observations about crystal shapes in bone tissue using electron microscopy and x-ray scattering techniques.[12, 14]

ACKNOWLEDGMENTS

The author is grateful to Profs. O. Penrose and J. L. Lebowitz for many discussions about Voronoi and hexagonal tesselations, as well as to Drs. N. Fratzl-Zelman and K. Klaushofer for their collaboration in the investigation of bone structure by x-ray scattering.

REFERENCES

1. M. J. Glimcher, In *Handbook of Physiology 7: Endocrinology*, **B2**:25, R. O. Greep and E. B. Astwood, eds. (American Physiological Society, Washington, D. C., 1976).
2. A. S. Posner, *Bone Mineral Res.* **5**:65 (1987).
3. E. Bonucci, *Calcification in Biological Systems* (CRC Press, Boca Raton, Florida, 1992).
4. W. J. Landis, *J. Ultrastruct. Mol. Struct. Res.* **94**:217 (1986).
5. A. L. Arsenault, *Bone Mineral* **6**:165 (1989).
6. W. Traub, T. Arad, and S. Weiner, *Proc. Natl. Acad. Sci. USA* **86**:9822 (1989).
7. S. Weiner and W. Traub, *Connective Tiss. Res.* **21**:259 (1989).
8. D. D. Lee and M. J. Glimcher, *J. Mol. Biol.* **217**:487 (1991).
9. W. J. Landis, M. J. Song, A. Leith, L. McEwen, and B. F. McEwen, *J. Struct. Biol.* **110**:39 (1993).
10. M. D. Grynpas, L. C. Bonar, and M. J. Glimcher, *J. Materials Sci.* **19**:723 (1984).
11. R. Legros, N. Balmel, and G. Bonel, *Calcif. Tiss. Int.* **41**:137 (1987).
12. A. L. Arsenault and M. D. Grynpas, *Calcif. Tiss. Int.* **43**:219 (1988).
13. P. Fratzl, N. Fratzl-Zelman, K. Klaushofer, G. Vogl, and K. Koller, *Calcif. Tiss. Int.* **48**:407 (1991).
14. P. Fratzl, M. Groschner, G. Vogl, H. Plenk, Jr., J. Eschberger, N. Fratzl-Zelman, K. Koller, and K. Klaushofer, *J. Bone Mineral Res.* **7**:329 (1992).
15. P. Fratzl, N. Fratzl-Zelman, and K. Klaushofer, *Biophys. J.* **64**:260 (1993).

16. S. W. White, D. J. S. Hulmes, A. Miller, and P. A. Timmins, *Nature* **266**:421 (1977).
17. L. C. Bonar, S. Lees, and H. A. Mook, *J. Mol. Biol.* **181**:265 (1985).
18. A. L. Boskey, N. Pleshko, S. B. Doty, and R. Mendelsohn, *Cells Materials* **2**:209 (1992).
19. S. Lees and E. A. Page, *Connective Tiss. Res.* **28**:263 (1992).
20. S. Lees and K. Prostak, *Connective Tiss. Res.* **18**:41 (1988).
21. H. J. Hoehling, R. H. Barckhaus, E. R. Krefting, J. Althoff, and P. Quint, In *Ultrastructure of Skeletal Tissues*, E. Bonucci and P. M. Motta, eds. (Kluwer, 1990), p. 41.
22. A. Guinier and G. Fournet, *Small-Angle Scattering of X-Rays* (Wiley, New York, 1955).
23. G. Porod, *Kolloid Z.* **124**:83 (1951); **125**:51 (1952).
24. P. Fratzl, *Acta Phys. Polon. A* **82**:121 (1992).
25. J. D. Gunton, M. San Miguel, and P. S. Sahni, In *Phase Transitions and Critical Phenomena*, C. Domb and J. L. Lebowitz, eds. (Academic Press, New York, 1983).
26. K. Binder, In *Materials Science and Technology*, P. Haasen, ed. (VCH, Weinheim, 1991), Vol. 5, Chapter 7, p. 405.
27. P. Fratzl and J. L. Lebowitz, *Acta Metall.* **37**:3245 (1989).
28. P. Fratzl, J. L. Lebowitz, O. Penrose, and J. Amar, *Phys. Rev. B* **44**:4794 (1991).
29. P. Fratzl, *J. Appl. Cryst.* **24**:593 (1991).
30. F. Langmayr, P. Fratzl, and G. Vogl, *Acta Metall. Mater.* **40**:3381 (1992).
31. D. Stoyan, W. S. Kendall, and J. Mecke, *Stochastic Geometry and Its Applications* (Wiley, New York, 1987), Chapter 10.
32. E. W. Kaler and S. Prager, *J. Colloid Interface Sci.* **86**:359 (1982).
33. H. Brumberger and J. Goodisman, *J. Appl. Cryst.* **16**:83 (1983).